Heliyon 5 (2019) e01966

Contents lists available at ScienceDirect

Heliyon

journal homepage: www.heliyon.com

Heliyon

A fluidized-bed reactor for the photocatalytic mineralization of phenol on TiO_2-coated silica gel

Guillermo J. Rincón [a,*], Enrique J. La Motta [b]

[a] Department of Civil & Environmental Engineering, University of New Orleans, 2000 Lakeshore Drive, Engineering Building, Room 817, New Orleans, LA, 70148, USA
[b] Edward G. Schlieder Urban Waste Management and Research Professor and Chair, Department of Civil and Environmental Engineering, University of New Orleans, 2000 Lakeshore Drive, Engineering Building, Room 815, New Orleans, LA, 70148, USA

ARTICLE INFO

Keywords:
Chemical engineering
Civil engineering
Photocatalysis
Fluidized bed reactor
Phenol mineralization
Anatase TiO_2
Silica gel

ABSTRACT

TiO_2 photocatalysis represents a promising class of oxidation techniques that are intended to be both supplementary and complementary to the conventional approaches for the removal of refractory and trace organic contaminants in water and air. Powdered TiO_2 dispersion systems employed in most studies require an additional separation step to recover the catalyst from the effluent water, which represents a major drawback for large scale applications. The optimization of photocatalytic treatment systems involves merging the benefits of catalyst immobilization on a retainable support, thus eliminating the need for downstream catalyst separation, maximization of photon-exposed catalyst area, and continuous operation.

Aiming to integrate such conditions into a single system, a bench-scale annular photo-reactor with concentric UV-C lamp was built to study the photocatalytic mineralization of phenol on fluidized silica gel beads coated with sol-gel-synthetized TiO_2. Reactor efficiency was investigated for different silica particle diameters (224, 357 and 461 μm), fluidized-bed concentrations in the bulk liquid (5, 10, 20 and 30 g L^{-1}), initial phenol concentrations in the aqueous solution (0.25 mmol L^{-1} to 4.0 mmol L^{-1}), and single and multiple sol-gel depositions. Then, the resulting optimum reactor configuration was compared to that of the same process on suspended Degussa P25 TiO_2 nanoparticles under similar experimental conditions. The latter is expected to be more efficient, but post-treatment catalyst recovery, being an energy intensive process, represents a major limitation for large scale applications. Process efficiency was measured as a function of the accumulated energy necessary for the mineralization of 50% of the initial dissolved chemical oxygen demand (COD), or, $Q_{0.5}$. Results showed that for any given mass of fluidized bed material, photo-oxidation efficiency increases with decreasing particle size (even for bed concentrations with similar equivalent surface area), decreasing initial phenol concentrations, and increasing number of sol-gel coatings. It was found that, for any given particle size and contaminant mass, there is an optimum bed concentration of 20 g L^{-1} for which $Q_{0.5}$ reaches a minimum. Finally, under the optimum configuration, the fluidized-bed reactor efficiency is only 30% lower than that of photocatalysis on suspended TiO_2 nanopowder, thus making the proposed fluidized system a viable alternative to slurry-TiO_2 reactors.

1. Introduction

TiO_2 photocatalysis represents a promising class of oxidation technique that is intended to be both supplementary and complementary to the conventional approaches for the removal of refractory and trace organic contaminants in water and air [1, 2, 3, 4]. Light-induced redox reactions take place on or near the surface of a catalyst and unselectively oxidize the contaminants into non-toxic products such as water, CO_2, and simple mineral acids [5, 6, 7].

Being a surface-mediated process, photocatalysis requires a high surface area to yield efficient degradation of dissolved contaminants. Typical photocatalytic treatment systems employ dispersions of powdered-TiO_2 with average particle size of 25 nm, which offer a high surface-to-mass ratio but normally require post-treatment separation. Such a requirement represents a major limitation for large scale applications as catalyst recovery is generally an energy intensive process, increasing overall capital and operational costs [8, 9]. In solar induced decontamination systems, for example, the cost requirement for post-treatment recovery of catalyst particles may even invalidate altogether the amount of energy savings claimed for such a process [10].

* Corresponding author.
E-mail address: gjrincon@uno.edu (G.J. Rincón).

https://doi.org/10.1016/j.heliyon.2019.e01966
Received 13 June 2018; Received in revised form 8 March 2019; Accepted 13 June 2019

As an alternative to slurry-type systems, the photocatalyst may be immobilized onto a support material such as quartz, glass, zeolite, or silica gel, eliminating or minimizing the need for downstream removal [8, 11, 12, 13, 14]. However, catalyst immobilization is not without shortcomings; for instance, it results in a much lower surface-to-mass ratio, which restricts processing capacities due to possible mass transfer limitations [15, 16].

Efficient immobilized photocatalyst systems require optimal irradiation of the fixed catalyst, along the possibility to operate continuously. Since photocatalytic reactions are local, i.e., they require the triple encounter of the surface, the reactant(s) and the photon(s) [17], photocatalytic reactor design must be based on maximization of the irradiated catalyst surface in contact with the dissolved contaminant.

One way to combine the benefits of catalyst immobilization and the need for irradiation optimization and continuous operation is through bed fluidization of a catalyst-coated support material. As reported by others [18], fluidized-bed reactors can improve efficiency of advanced-oxidation processes used for contaminant removal from water, by eliminating waste and the need for post-treatment. Prevailing limitations of such configuration include the lack of understanding of the effects of reactor geometry on process efficiency and treatment cost.

The research reported herein presents the results of photocatalytic experiments for the oxidation of phenol in a bench-scale annular fluidized-bed batch reactor with a concentric UV-C lamp and anatase TiO_2-coated silica gel beads as bed material. Previous studies on reactors with similar configuration have focused primarily on evaluating catalyst synthesis and stability, and overall system photocatalytic activity [19]. However, little has been done to assess the impact of important parameters related to reactor and bed characteristics. Therefore, this paper aims to evaluate the effect of so-far-overlooked operational variables, such as bed particle size and concentration, and reactor geometry, on energy expenditure during mineralization of varying contaminant loads. Experimental data analysis was used for establishing an optimum configuration of the fluidized bed reactor, and then its photocatalytic efficiency compared to that of suspended P25 TiO_2 under similar experimental conditions.

2. Experimental

2.1. Photocatalytic reactor

A photocatalytic treatment system consisting of a stainless-steel tubular batch reactor equipped with a concentric UV-C lamp, shown in Fig. 1a and b, was built to the specifications presented in Table 1. The design satisfied the following criteria: easy implementation in a laboratory setting, complete and uniform fluidization of the bed material throughout the bulk reactor volume by means of fluid recirculation, uniform light distribution across the liquid bulk, ready connection to a compressed-oxygen source, easy replacement of bed material, and accessible sampling ports.

Stainless steel 316 was used for all parts of the reactor, which consists of a vertical tube 457-mm long, with an inside diameter of 50.8 mm, and a total inner volume of 800 ml. A UV-C lamp (LMP-GPH436T5L/HO/4PSE) with a nominal output of 120 μW cm^{-2} at 254 nm served as the light source. The lamp was placed concentrically inside the reactor and encased in a high clarity quartz sleeve with an external diameter of 25.4 mm, yielding a reactor annular area of 1.6×10^{-3} m^2.

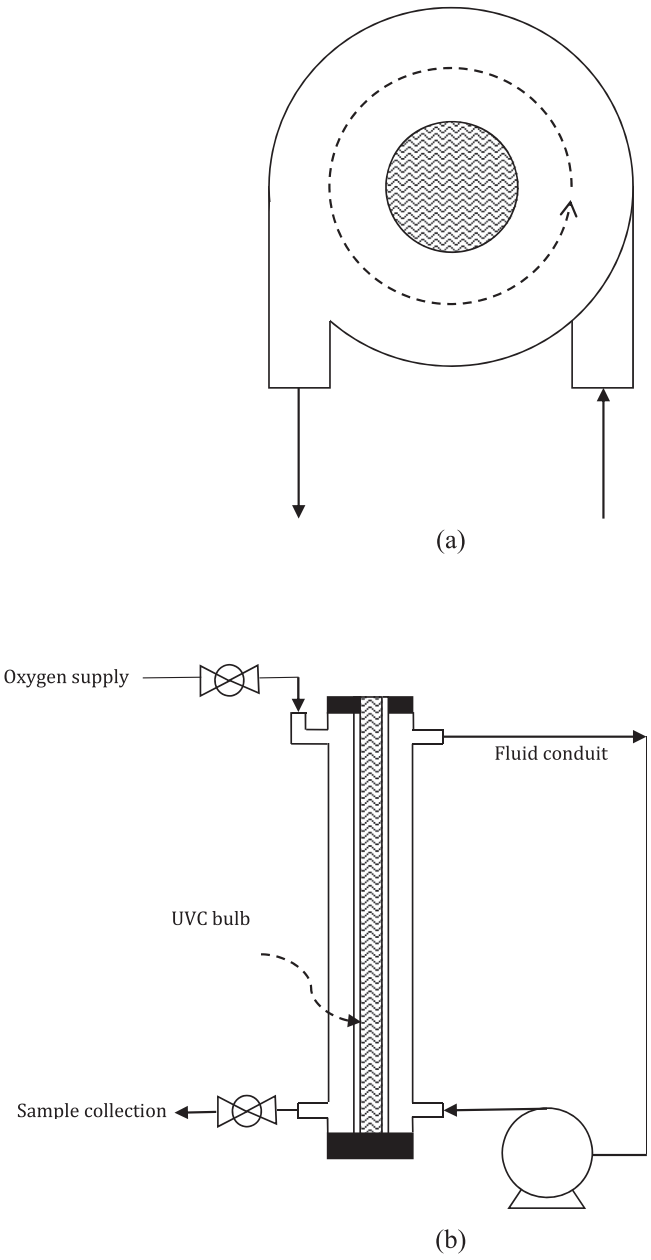

Fig. 1. (a) Plan view of the photocatalytic reactor showing the placement of inlet and outlet ports, and fluid circulation pattern. (b) Elevation view of the photocatalytic treatment system showing the placement of inlet, outlet and oxygen supply ports, and fluid conduits.

The irradiated length, which corresponds to the arc section of the lamp submerged in liquid, was 375 mm which results in an effective (or irradiated) volume of 600 mL. The intensity of irradiated UV-C light perpendicular to the surface of the lamp was measured with a UV sensor (Cole Parmer Digital Radiometer UVX-25).

A stainless-steel fitting was installed at the top of the reactor for

Table 1
Specifications and characteristic parameters of photocatalytic reactor.

Parameter		Parameter	
Reactor inside diameter	50.8 mm	Irradiated length (L_R)	375 mm
Bulb case outside diameter	25.4 mm	Irradiated surface area (A_R)	14962 mm^2
Annular area	1600 mm^2	Irradiated volume (V_R)	600 ml
Annular area width	12.7 mm	Irradiance at A_R (E_R)	25 mW cm^{-2}
Total volume (V_T)	800 ml	Radiant power at A_R (Φ_R)	3740 mW

feeding oxygen from a compressed-oxygen tank, thus creating a pressurized headspace above the bulk liquid in the reactor. Inlet and outlet ports were placed perpendicularly and tangentially to the surface of the tube (Fig. 1a), with inlet at the bottom and outlet at the top, thus forcing the liquid to flow in an upward helical pattern. A peristaltic pump (Cole Parmer Masterflex I/P modular analog pump with benchtop controller, model 77601–10) was used for fluid recirculation.

2.2. Photocatalyst synthesis and silica gel coating

Bed material consisted of high-purity grade silica gel particles (SiO_2, Davisil Grade 636) size range 250–500 μm (35–60 mesh) supplied by Sigma Aldrich. Photocatalytic experiments were performed using sieve-separated particles retained in 0.200-mm, 0.300-mm, and 0.425-mm sieves with mean geometric diameters of 0.224 mm, 0.357-mm, and 0.461 mm, respectively. By running a clear-wall acrylic replica of the experimental reactor, it was confirmed that silica gel beds of any of the evaluated sizes and concentrations fully fluidized throughout the annular volume in the experimental flow rate (8.9×10^{-6} $m^3 s^{-1}$, equivalent to a velocity of 5.6×10^{-3} ms^{-1} through the reactor annular space), while also allowing for rapid particle settling after shutting the pump off.

For any silica gel sample, bed porosity (ε) in water was calculated to be 0.45, with an approximate pore volume of 0.95 mL g^{-1} of silica gel. A sphericity factor (φ) of 0.78 was assumed for the silica gel beads due to its irregular shape. The external silica surface area was found using Eq. (1):

$$A_m = \left(\frac{\text{Pore volume}}{\varphi}\right)\left[\frac{6(1-\varepsilon)}{\varepsilon\, d}\right] \quad (1)$$

where d represents the mean geometric diameter of the silica beads. Table 2 shows the external surface area per unit mass for the different particle diameters used for catalyst support as calculated with Eq. (1).

A common sol-gel technique selected for its simplicity and economical implementation was used to synthetize and deposit TiO_2 on the silica gel particles [20, 21]. 2.7 mL of concentrated HCl were added into a mixture containing 15 ml of titanium (IV) isopropoxide (98+% by Acros Organics) and 100 mL of absolute ethanol. A 100-mL beaker containing silica gel beads was placed in a 300-mL beaker containing ethanol, then covered with a watch glass and warmed at 80 °C for 1 h. Silica gel beads were washed with ethanol, immersed in the precursor solution for 90 min, filtered using suction, and dried at 110 °C following drying at room temperature overnight. The beads were then heated in an electric furnace at 450 °C for 3 h. The amount of TiO_2 anchored onto the silica beads could be increased by subjecting the beads to repeated coating treatments. Batches of silica gel coated with one, two and three sol-gel layers were prepared. The morphology of the photocatalyst layer after three consecutive depositions was examined by scanning electron microscopy (Carl Zeiss LEO 1530VP-FESEM) and is shown in Fig. 2.

2.3. Photocatalytic experiments

In a typical photocatalytic experiment, the reactor was loaded with a known amount of coated silica gel beads and 800 mL of an unbuffered phenol aqueous solution of a prescribed concentration. The resulting mixture was then recirculated at the minimum rate that produced complete bed fluidization, or 8.9×10^{-6} m^3 s^{-1} (530 mL min^{-1}), and saturated with oxygen by contact with a pure-oxygen headspace.

Table 2
External surface area per unit mass for different silica gel particle diameters.

Geometric mean diameter (d), m	Hydraulic radius of silica beads (R), m	External silica surface area per gram (A_m), m^2 g^{-1}
2.24E-04	2.38E-05	3.99E-02
3.57E-04	3.80E-05	2.50E-02
4.61E-04	4.90E-05	1.94E-02

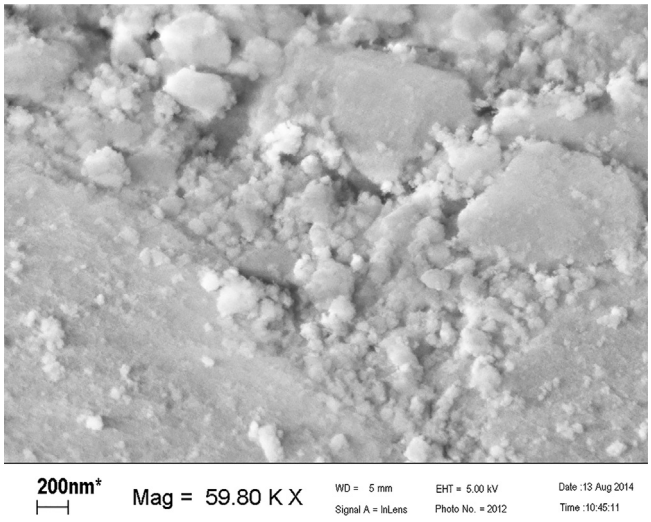

Fig. 2. SEM image showing morphology of sol-gel deposited TiO_2 (anatase).

Temperature of the mixture was not controlled but allowed to vary freely during the experiments.

The mixture was recirculated in the dark for an hour to allow for adsorption equilibrium. Then, UV-C irradiation was initiated by placing the lamp inside the quartz casing. 30-mL samples were taken at 30-minute intervals throughout the 8-hours-long experiment. Temperature, pH, and dissolved oxygen concentration (DO) were measured immediately after sample collection with Thermo-Scientific Orion probes and multimeter. Then, the sample was filtered through a 0.45-μm cellulose nitrate filter (Whatman Ltd.) to remove suspended and colloidal matter (Standard Method 5910 for Determination of UV-C Absorbing Organic Constituents). After filtration, COD was measured using a UV-Vis Spectrophotometer (Hach DR 5000) according to the USEPA Reactor Digestion Method (Method 8000) with Hach TNT Plus 822 and 821 vials for high and low range COD concentrations, respectively. Test accuracy is ±2% for high range and ±5% for low range COD determination. In this research, COD was used as indicator of contaminant load. Control experiments consisted of adsorption in the dark, photolysis, and simultaneous photolysis and adsorption.

The optimal bed load and silica bead size were determined by varying the mass (5, 10, 20 and 30 g L^{-1}) and size (224, 357 and 461 μm) of the catalyst-coated silica beads in the mixture. The effect of the number of sol-gel depositions and initial phenol concentration on the photocatalytic efficiency of the system was assessed by using particles with one and three catalyst layers and by varying the initial phenol concentrations from 0.25 mmol L^{-1} to 4.0 mmol L^{-1}, respectively. Finally, the fluidized-bed reactor performance was compared to that of the same reactor operated in slurry-mode with a 1.25-g L^{-1} P25 TiO_2 suspension (anatase nano-powder, particle size <25 nm, 99.7% trace metals basis by Sigma Aldrich). This amount is equivalent to the mass of TiO_2 deposited on 20 g L^{-1} of silica particles after a single sol-gel deposition.

The efficiency of the photocatalytic system is expressed herein as the accumulated energy, Q_{UV}, in kJ L^{-1}, required for partial mineralization, as proposed by others [22]. This parameter, as per Eq. (2), takes into consideration the radiant power densityE_R, reaching the surface area of exposed catalyst, A_R, as related to the total reactor volume, V_T:

$$Q_{UV,n} = Q_{UV,\,n-1} + \Delta t_n E_R \frac{A_R}{V_T} \quad (2)$$

where Δt_n is the differential experimental time. Values of E_R, A_R and V_T for the experimental reactor are presented in Table 1. Since the product of radiant power density and irradiated surface area yields the radiant power, Φ_R, Eq. (2) can be rewritten as:

$$Q_{UV,n} = Q_{UV,\,n-1} + \Delta t_n \frac{\Phi_R}{V_T} \quad (3)$$

Thus, by measuring the elimination of COD with irradiation time, the accumulated energy necessary for the mineralization of 50% of the initial dissolved COD, or $Q_{0.5}$, can be calculated from Eq. (3).

3. Results and discussion

3.1. Effect of concentration and size of silica gel particles

Experimental results indicate that both bed concentration (bed mass per unit volume of mixture) and silica particle size affect the photocatalytic efficiency of the system by either limiting reactive sites availability or contributing to the apparent turbidity of the mixture.

Typical experiments performed using four different bed concentrations (5, 10, 20 and 30 g L^{-1}) and three silica beads sizes (224, 357 and 461 μm) coated with a single catalyst layer demonstrate such effect on the accumulated energy, $Q_{0.5}$, as shown in Fig. 3. Here, for any given particle size, there is an optimum bed concentration of 20 g L^{-1} for which $Q_{0.5}$ reaches a minimum and increases for lower and higher concentrations of coated particles in the mixture.

A similar behavior can be observed in Fig. 4, where accumulated energy is plotted against equivalent surface area of coated silica per unit volume of mixture, or bed surface area concentration (calculated from Table 2). Fig. 4 shows that there is an ideal surface area concentration that yields a maximum efficiency for each of the different experimental particle sizes, and also that as particle size increases, not only photocatalytic efficiency decreases, but also the magnitude of change in $Q_{0.5}$ becomes larger for other-than-optimum bed concentrations.

The decreased efficiency observed in the case of lower-than-optimum bed concentration is indicative of system exhaustion, or the hindering of the photo-oxidation capability of the system owing to saturation and reduced photonic activation of the catalyst surface produced by an excessive substrate concentration relative to the available photogenerated active sites. In the case of higher-than-optimum bed concentrations, the light blocking effect of particles overload is likely responsible for the decreased catalyst activation rate.

The observed influence of catalyst surface area on degradation rate also provides clues of the type of photo-oxidation mechanism prevalent for this type of system. It has been reported that for compounds that can react by direct electron transfer, the removal rate decreases with the surface area. The opposite occurred for compounds prone to react through $OH^{\bullet}$ radical-mediated attack [23, 24]. Also, the photo-redox chemistry that occurs at the semiconductor surface is emanated from trapped electrons and trapped holes rather than from free valence band holes and conduction band electrons [25], which confirms the surface-bound nature of the interactions between trapped covalent band electrons and valence band holes, and the bulk liquid as suggested by the

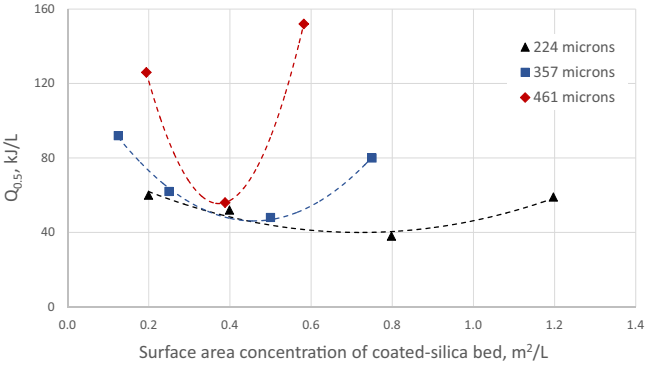

Fig. 4. $Q_{0.5}$variation with bed surface-area concentration (Single deposition on 224-μm, 357-μm and 461-μm particles, 1.0 mmol L^{-1} initial phenol concentration).

experimental results. Therefore, either by direct substrate oxidation, trapped electron-hole generation of oxidative radicals, or a combination of both mechanisms, the photocatalytic oxidation of phenol is limited by the catalyst surface area available for active sites formation, and accessible by contaminants and photons. In such scenario, mass transfer phenomena would play a secondary, non-limiting role.

3.2. Effect of initial phenol concentration

In photocatalytic studies on phenol oxidation in oxygenated solutions with TiO_2 powder in suspension, high initial phenol concentrations have been reported to negatively affect the pseudo-first order reaction rate constant, producing an inhibitory effect on the apparent rate constant, or that phenol mineralization decreased with increasing initial phenol concentration [26, 27, 28, 29]. In the case of the fluidized-bed reactor with coated bed material used in this research, the combined effect of both phenol and bed concentration in the mixture was studied through typical photocatalytic experiments varying the initial phenol concentration from 0.5 to 2.0 mmol L^{-1} for different bed concentrations using 357-μm-silica particles with a single TiO_2 layer. Results are summarized in Figs. 5 and 6.

These figures show that for any given bed or equivalent surface area concentration, photo-oxidation efficiency decreases as the initial phenol concentration increases. The effect of bed concentration on process efficiency is again evident, with 20 g L^{-1} of coated silica bed yielding the highest efficiency for initial phenol concentrations of 1.0 and 2.0 mmol L^{-1} and decreased $Q_{0.5}$ for other-than-optimal bed load. However, for very low phenol load (0.5 mmol L^{-1}), bed concentration appears to have no effect on the degradation rate.

This phenomenon has been attributed to the photonic nature of the photocatalytic reactions, which means that, at high enough contaminant

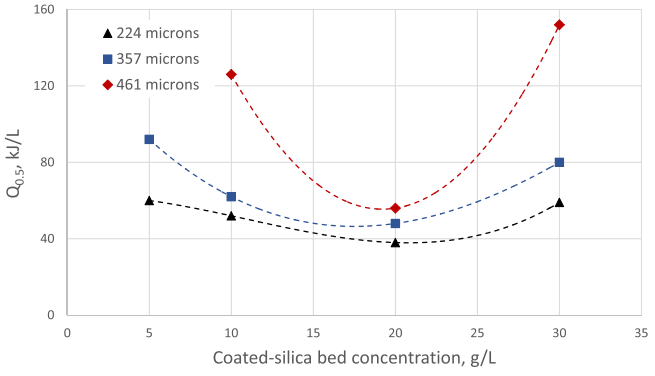

Fig. 3. $Q_{0.5}$ variation with particle bed concentration (Single deposition on 224-μm, 357-μm and 461-μm particles, 1.0 mmol L^{-1} initial phenol concentration).

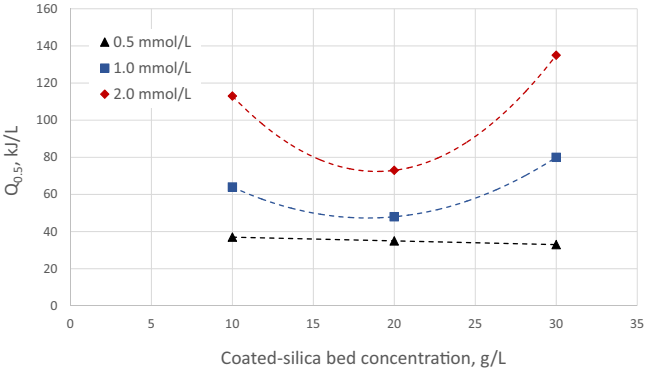

Fig. 5. $Q_{0.5}$ variation with particle bed concentration (0.5, 1.0 and 2.0 mmol L^{-1} initial phenol concentration, single deposition on 357-μm-particles).

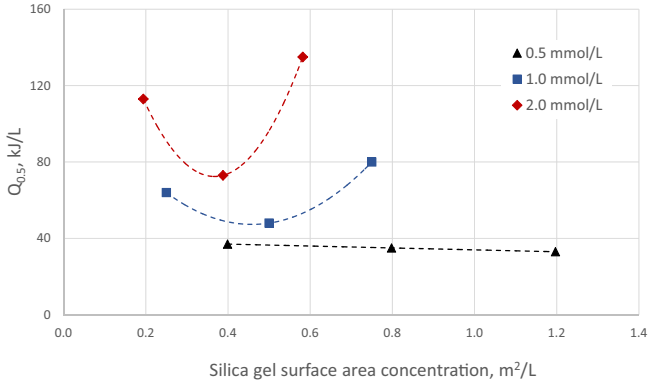

Fig. 6. $Q_{0.5}$variation with bed-surface-area concentration (0.5, 1.0 and 2.0 mmol L^{-1} initial phenol concentration, single deposition on 357-μm-particles).

concentrations, photocatalyst deactivation occurs due to the simultaneous saturation of the TiO_2 surface and reduction of the photonic efficiency [30, 31]. Some authors have proposed that such decrease in the reaction rate at high substrate concentration is due to the presence of back reactions [32, 33], scenario that considers the possibility of a substrate radical being able to inject an electron into the conduction band of the semiconductor surface [34].

3.3. Reactor performance comparison

The performance of the experimental fluidized-bed photocatalytic reactor was compared to that of the same reactor operated under different conditions. This was done with a dual purpose: (i) to demonstrate the improved removal efficiency of the proposed reactor compared to, for example, combined adsorption over clean silica gel and UV-photolysis, and (ii) to estimate the photocatalytic efficiency lost due to catalyst immobilization, by measuring the COD disappearance rate in an irradiated TiO_2 dispersion. Specifically, the reactor performance was evaluated for the following processes using a phenol aqueous solution with initial concentration of 1.0 mmol L^{-1}:

i) Adsorption only, by running an experiment "in the dark" with 20 mg L^{-1} of uncoated 357-μm-silica particles.
ii) Photolysis only, by UV-C irradiation of the phenol solution in the absence of any photocatalyst-coated-silica particles.
iii) Combined photolysis and adsorption, through a typical experiment using 20 g L^{-1} of uncoated 357-μm-silica particles.
iv) Slurry-mode photocatalysis, by UV-C irradiation of a suspension containing 1.25 g L^{-1} of TiO_2 nano-powder. This amount is equal to the mass of TiO_2 deposited on 20 g L^{-1} of silica particles after a single sol-gel deposition.

Additional typical experiments were performed using the previously determined optimum bed concentration of 20 g L^{-1} and silica beads treated with three consecutive sol-gel depositions. Results showing the change in COD remaining fraction with time for different processes are summarized in Fig. 7.

Adsorption of phenol on the silica particles is low, and COD removal after 8 h of contact is negligible. On the other hand, photocatalysis with anatase nano-powder removes all the initial COD after only 4 h of irradiation. Photolysis was slightly more efficient than combined photolysis and adsorption on uncoated silica, evidencing the light-blocking effect of the fluidized bed particles. Photocatalysis using a fluidized bed of tripled-coated silica particles was 100% more efficient than photolysis only in removing the initial COD after 8 h of treatment.

By conducting experiments similar to the ones depicted in Fig. 7 for varying initial phenol concentrations, it is possible to determine the influence of contaminant load on the reactor performance measured as the

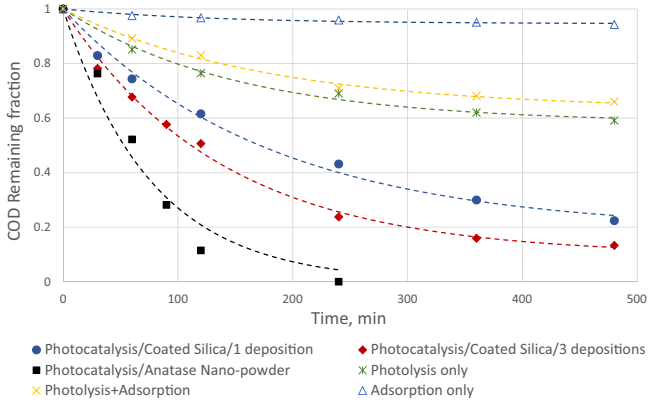

Fig. 7. COD decay profile in a 1.0 mmol L^{-1} phenol solution for different processes.

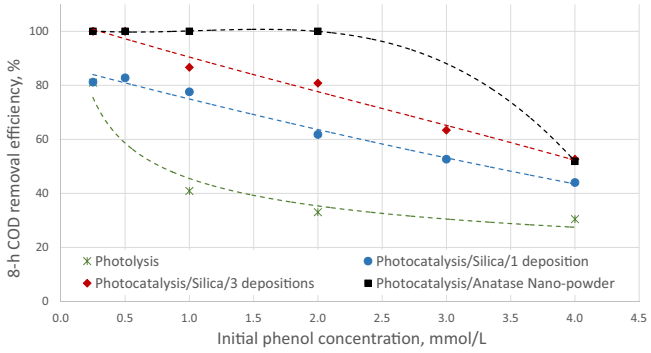

Fig. 8. 8-h COD removal efficiency variation with initial phenol concentration for different photo-oxidation processes.

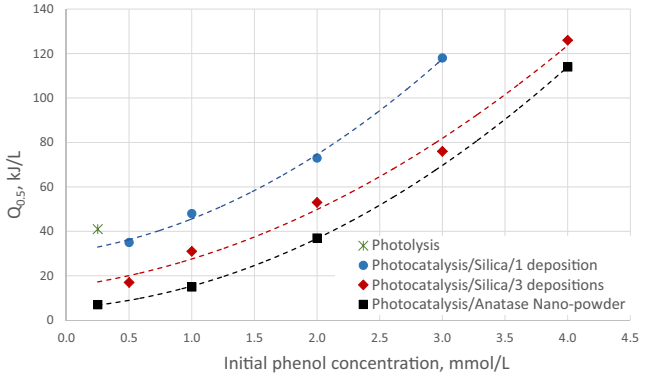

Fig. 9. $Q_{0.5}$ variation with initial phenol concentration for different photo-oxidation processes.

COD removal after 8 h of irradiation (8-h COD) and $Q_{0.5}$. Corresponding results are presented in Figs. 8 and 9.

According to Fig. 8, the maximum photocatalytic efficiency in the experimental reactor is achieved in slurry-mode using TiO_2 nano-powder. This process removes all the phenol-derived COD for initial concentrations lower than 2.0 mmol L^{-1}. The 8-h removal efficiency decreases for higher substrate concentrations. Also, at very low (0.25 mmol L^{-1}) and very high (4.0 mmol L^{-1}) initial phenol concentrations, photocatalysis on TiO_2 powder is as efficient at removing COD as the photocatalysis on fluidized silica particles with three layers of catalyst. Fig. 8 also shows that at very low contaminant concentrations, photolysis and photocatalysis on silica with a single deposition yield the same COD removal.

A similar trend is observed in Fig. 9, where the $Q_{0.5}$ increases with

phenol concentration for all the compared processes. When measuring photocatalytic efficiency as a function of energy consumption, photocatalysis on suspended TiO_2 particles is in average 50% and 30% more efficient than the same process on the fluidized bed of silica beads with one and three layers of catalyst, respectively, for all the experimental initial phenol concentrations. Photolysis can only achieve the half-concentration point at the very low initial phenol concentration of 0.25 mmol L^{-1}.

4. Conclusions

The photocatalytic elimination of phenol-derived COD in the experimental fluidized-bed tubular reactor is significantly affected by the size and concentration of the catalyst support in the bulk mixture. Results show that for any given mass of fluidized bed, efficiency increases with decreasing particle size, suggesting that catalysts with lower surface area provide lower mineralization rates, and that high catalyst surface area is beneficial as it provides higher concentration of active sites per surface unit, thus leading to superior reactivity. However, as shown in this study, even for the same surface area concentration, process efficiency decreases with increasing particle diameter, indicating that the particle size has a direct influence on photon efficiency by producing a blocking effect between the light source and the catalyst surface. Additionally, it was demonstrated that, for the experimental tubular fluidized-bed reactor with concentrical lamp, an excess of particles can create a light shielding effect which reduces the catalyst surface area being exposed to illumination. Therefore, an optimum bed concentration of 20 g of coated silica beads per liter of mixture was observed to maximize degradation efficiency while minimizing energy expenditure.

Results also indicate that photocatalytic degradation rate of COD decreases with increasing initial phenol concentrations over the entire experimental range of particle sizes, bed loads and number of TiO_2 layers. In the case of phenol, photo-oxidation intermediate compounds increase the time and energy necessary for COD elimination owing to the direct competition over limited unselective reactive sites on the catalyst surface and to the reduction in photon efficiency caused by the increased absorbance of the irradiated mixture.

Additional layers of TiO_2 on the support particle increases photocatalytic efficiency by improving catalyst surface availability for photon absorption and substrate oxidation. This is an important factor in photocatalytic reactions, where organic substrates can be oxidized both directly by trapped holes and indirectly by surface-adjacent radicals, thus requiring the confluence of catalyst, photons and substrate.

When comparing the reactor performance for the different processes evaluated, the maximum efficiency was obtained in slurry-mode using a 1.25-g L^{-1} suspension of P25 TiO_2 nano-powder. In general, for initial phenol concentrations between 0.5 and 4 mmol L^{-1}, the $Q_{0.5}$ of photocatalysis on P25 TiO_2 is in average 50% lower than the $Q_{0.5}$ of photocatalysis on a fluidized bed of 357-μm-particles with a single sol-gel deposition, and 30% lower for 357-μm-particles with three consecutive depositions. However, COD removal efficiency is similar for the P25 suspension and the fluidized-bed system using 357-μm-particles with three depositions at phenol concentrations as low as 0.25 mmol L^{-1}. On the other end of the spectrum, at high phenol concentrations, substrate oxidation by photocatalysis becomes ineffective and energy intensive for any configuration.

Although optimization of catalyst stability and photon efficiency are necessary to improve reactor performance, the proposed photocatalytic system demonstrates the feasibility of photo-oxidizing dissolved pollutants in fluidized bed reactors at a rate comparable to that of slurry-type systems, specially at the low concentrations range normally found in drinking water. This combined with the advantage of catalyst retention and reuse, and the possibility of employing visible-light active photocatalysts, make these type of reactors a viable, sustainable alternative to other more energy intensive advanced-oxidation methods.

Declarations

Author contribution statement

Guillermo Rincon: Conceived and designed the experiments; Performed the experiments; Analyzed and interpreted the data; Contributed reagents, materials, analysis tools or data; Wrote the paper.

Enrique La Motta: Analyzed and interpreted the data; Contributed reagents, materials, analysis tools or data.

Funding statement

This research did not receive any specific grant from funding agencies in the public, commercial, or not-for-profit sectors.

Competing interest statement

The authors declare no conflict of interest.

Additional information

No additional information is available for this paper.

References

[1] L. Favier, A. Simion, E. Matei, C. Grigoras, Y. Kadmi, A. Bouzaza, Photocatalytic oxidation of a hazardous phenolic compound over TiO_2 in a batch system, Environ. Eng. Manag. J. 15 (5) (2016) 1059–1067.

[2] A. Abeish, H. Ang, H. Znad, Solar photocatalytic degradation of chlorophenols mixture (4-CP and 2,4-DCP): mechanism and kinetic modelling, J. Environ. Sci. Health - Part A Toxic/Hazard. Subst. Environ. Eng. 50 (2) (2015) 125–134.

[3] O. Alfano, D. Bahnemann, A. Cassano, R. Dillert, R. Goslich, Photocatalysis in water environments using artificial and solar light, Catal. Today 58 (2000) 199–230.

[4] Z. Ding, H.Y. Zhu, G.Q. Lu, P.F. Greenfield, Photocatalytic properties of titania pillared clays by different drying methods, J. Colloid Interface Sci. 209 (1) (1999) 193–199.

[5] S. Malato, J. Blanco, A. Vidal, C. Richter, Photocatalysis with solar energy at a pilot-plant scale: an overview, Appl. Catal. B Environ. 37 (1) (2002) 1–15.

[6] J.C. Crittenden, J. Liu, D.W. Hand, D.L. Perram, Photocatalytic oxidation of chlorinated hydrocarbons in water, Water Res. 31 (3) (1997) 429–438.

[7] M.R. Hoffmann, S.T. Martin, W. Choi, Environmental applications of semiconductor photocatalysis, Chem. Rev. 95 (1995) 69–96.

[8] J.A. Byrne, A. Davidson, P.S.M. Dunlop, B.R. Eggins, Water treatment using nanocrystalline TiO_2 electrodes, J. Photochem. Photobiol. A Chem. 148 (2002) 365–374.

[9] J.A. Byrne, B.R. Eggins, N.M.D. Brown, B. McKinley, M. Rouse, Immobilization of TiO_2 powder for the treatment of polluted water, Appl. Catal. B Environ. 17 (1998) 25–36.

[10] R.L. Pozzo, M.A. Baltanas, A.E. Cassano, Supported titanium dioxide as photocatalyst in water decontamination: state of the art, Catal. Today 39 (1997) 219–231.

[11] S. Ray, J. Lalman, Fabrication and characterization of an immobilized titanium dioxide nanofiber photocatalyst, Mater. Today: Proceedings 3 (6) (2016) 1582–1591.

[12] R.M. Abhang, D. Kumar, S.V. Taralkar, Design of photocatalytic reactor for degradation of phenol in wastewater, Int. J. Chem. Eng. Appl. 2 (5) (2011) 337–341.

[13] R.F.P. Nogueira, W.F. Jardim, TiO_2-fixed-bed reactors for water decontamination using solar light", Sol. Energy 56 (5) (1996) 471–477.

[14] Y. Zhang, J.C. Crittenden, D.W. Hand, Fixed-bed photocatalyst for solar decontamination of water, Environ. Sci. Technol. 28 (1994) 435–442.

[15] R.W. Matthews, Photooxidative degradation of colored organics in water using supported catalysts: TiO_2 on sand, Water Res. 25 (1991) 1169–1176.

[16] C.S. Turchi, D.F. Ollis, Photocatalytic reactor design: an example of mass transfer limitations with an immobilized catalyst, J. Phys. Chem. 92 (1988) 6852–6853.

[17] M. Bideau, B. Claudel, C. Dubien, H. Kazouan, On the immobilization of titanium dioxide in the photocatalytic oxidation of spent waters, J. Photochem. Photobiol. A Chem. 91 (1995) 137–144.

[18] F. Tisa, A. Aziz-Raman, W. Ashri, Applicability of fluidized bed reactor in recalcitrant compound degradation through advanced oxidation processes: a review, J. Environ. Manag. 146 (2014) 260–275.

[19] W. Qiu, Y. Zheng, A comprehensive assessment of supported titania photocatalysts in a fluidized bed photoreactor: photocatalytic activity and adherence stability", Appl. Catal. B Environ. 71 (2007) 151–162.

[20] A. Hanel, P. Moren, A. Zaleska, J. Hupka, Photocatalytic activity of TiO_2 immobilized on glass beads, Physicochem. Prob. Miner. Processing. 45 (2010) 49–56.

[21] K. Kobayakawa, C. Sato, Y. Sato, A. Fujishima, Continous-flow photoreactor packed with titanium dioxide immobilized on large silica gel beads to decompose oxalic acid in excess water, J. Photochem. Photobiol. A Chem. 118 (1998) 65–69.
[22] M. Kositzi, I. Poulios, S. Malato, J. Caceres, A. Campos, Solar photocatalytic treatment of synthetic municipal wastewater, Water Res. 38 (2004) 1147–1154.
[23] A. Agrios, P. Pichat, Recombination rate of photogenerated charges vs. surface area: opposing effects of TiO_2 sintering temperature on photocatalytic removal of phenol, anisole and pyridine in water", J. Photochem. Photobiol. A Chem. 180 (2006) 130–135.
[24] R. Enriquez, P. Pichat, Different net effect of TiO_2 sintering temperature on the photocatalytic removal rates of 4-chlorobenzoic acid and dichloroacetic acid in water, J. Environ. Sci. Health A: Toxic/Hazardous Subst. Environ. Eng. 41 (2006) 955–966.
[25] N. Serpone, G. Sauve, R. Koch, H. Tahiri, P. Pichat, P. Piccinini, E. Pelizzetti, H. Hidaka, Standardization protocol of process efficiencies and activation parameters in heterogeneous photocatalysis: relative photonic efficiencies zeta(r), J. Photochem. Photobiol. A Chem. 94 (1996) 191–203.
[26] H.K. Singh, M. Saquib, M.M. Haque, M. Muneer, Heterogeneous photocatalyzed degradation of 4-chlorophenoxyacetic acid in aqueous suspensions, J. Hazard Mater. 142 (2007) 374–380.
[27] R. Alnaizy, A. Akgerman, Advanced oxidation of phenolic compounds", Adv. Environ. Res. 4 (2000) 233–244.
[28] T. Wei, C. Wan, Heterogeneous photocatalytic oxidation of phenol with titanium dioxide powders, Ind. Eng. Chem. Res. 30 (1991) 1293–1300.
[29] V. Augugliaro, L. Palmisano, A. Sclafani, C. Minero, E. Pelizzetti, Photocatalytic degradation of phenol in aqueous titanium dioxide dispersions, Toxicol. Environ. Chem. 16 (1988) 89–90.
[30] M.N. Chong, B. Jin, C.W.K. Chow, C. Saint, Recent developments in photocatalytic water treatment technology: a review", Water Res. 44 (2010) 2997–3027.
[31] M. Saquib, M. Muneer, TiO_2-mediated photocatalytic degradation of a triphenylmethane dye (gentian violet), in aqueous suspensions, Dyes Pigments 56 (2003) 37–49.
[32] C. Minero, D. Vione, A quantitative evaluation of the photocatalytic performance of TiO_2 slurries", Appl. Catal. B Environ. 67 (2006) 257–269.
[33] C. Minero, Kinetic analysis of photoinduced reactions of photoinduced reactions at the water semiconductor interface, Catal. Today 54 (1999) 205–216.
[34] T.L. Villarreal, R. Gómez, M. González, P. Salvador, A kinetic model for distinguishing between direct and indirect interfacial hole transfer in the heterogeneous photooxidation of dissolved organics on TiO_2 nanoparticle suspensions", J. Phys. Chem. B 108 (52) (2004) 20278–20290.